

4.1.2 X-Ray Diffraction Analysis (XRD)

The diffraction analyses of the samples were categorized into three divisions that are the pure samples (PVA, starches, and treated fibers), blends of PVA with different starches and blends of PVA with different starches and treated fibers. For the samples of pure starches, the crystalline type pattern of the starch was determined. Starches tend to present particular crystalline arrangements regarding their botanical origin. For starch, the presence of crystalline regions within its molecular structure is attributed to the ordered arrangements of adjacent double helix amylopectin branches. There are three recognized types of starch crystallinity patterns, and these are commonly designated as A-, B- and C-type crystals (Moharram, Abou-Samaha, & Bekheet, 1998). In the analysis of the tropical starch used in this study, the assignment of the three starches to any groups of crystal type were based on the direct comparison of the X-ray diffractograms with the diffractograms patterns of the starches that have been well established and characterized. For the samples of treated fibers, the crystallinity index of cellulose was determined using the method proposed by Segal et. al (Segal, Creely, Martin Jr., & Conrad, 1959). Using the data of the x-ray scanning, degree of crystallinity was calculated using the following equation:

$$Cr I = \frac{I_{002} - I_{am}}{I_{002}} \times 100$$

where

$Cr I$ = crystallinity index (%)

I_{002} = the maximum intensity (in arbitrary units) of the (002) lattice diffraction representing crystalline material

I_{am} = the intensity of the diffraction in the same units at $2\theta = 18^\circ$ (for cellulose I) representing amorphous material in cellulosic fibers.

By using the x-ray scanning data of the blended composite, crystallite width was determined by applying Scherrer equation (Alexander, 1969):

$$D = \frac{k \lambda}{\beta \cos \theta}$$

where

D = average crystallite width

k = constant (0.9)

λ = x-ray wavelength (1.5406 Å)

θ = Bragg's angle

β = breadth for (002) peak at half-peak intensity

Pure samples (PVA, different starches and different fibers)

Figure 4.19 shows the x-ray diffractogram of pure PVA in casted film form. Pure PVA exhibits two distinct peaks that are $2\theta = 19.8^\circ$ and 22.5° corresponding to its crystalline structure. The d values (interplanar spacing) associated with these peaks are 4.48 and 3.95 Å (Pal, Banthia, & Majumdar, 2006)(Pal, Banthia, & Majumdar, 2008).

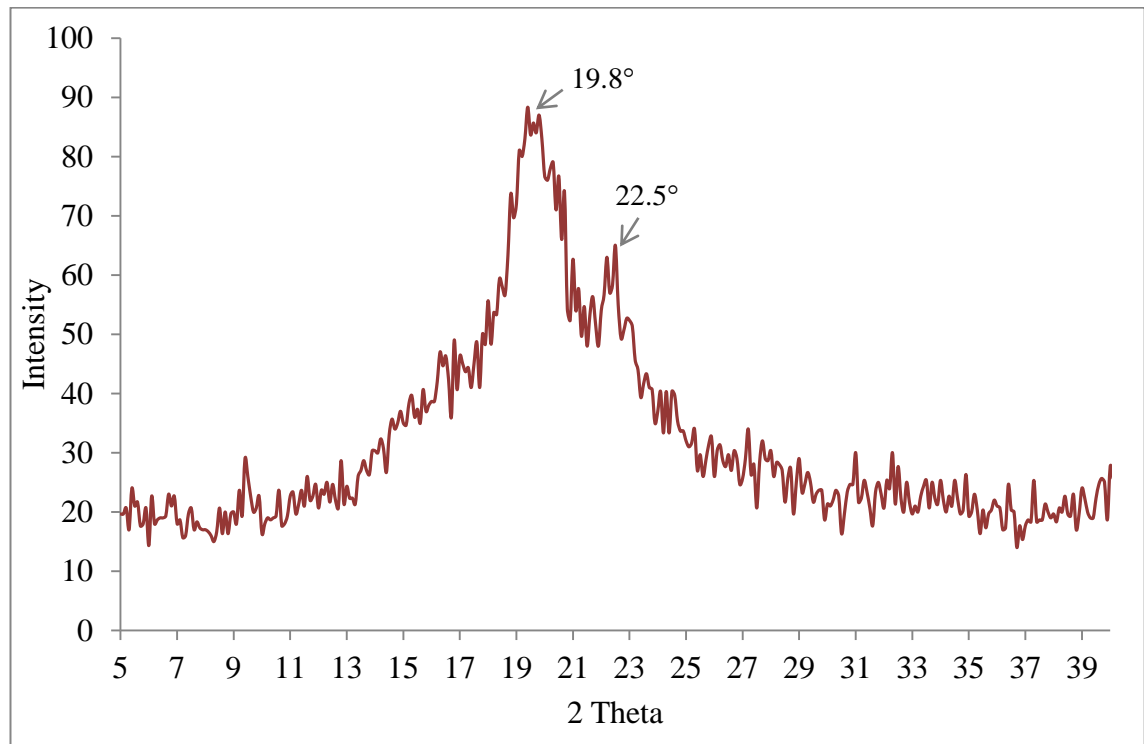


Fig. 4.19 X-ray diffraction pattern of pure PVA

The x-ray diffractograms of the three different tropical starches (tapioca, rice and sago starch) are presented in Figure 4.20. When compared to the diffraction peaks of characteristics crystal pattern of different types of crystals in starches, the patterns of the diffraction peaks of the tapioca and sago starch used in this study resembles the diffraction peaks that are characteristic of the C-type crystal pattern of starch (Pickard, Asaoka, & Blanshard, 1991) (Moorthy, Wenham, & Blanshard, 1996) (DeFloor, Dehing, & Delcour, 1998) (Galant, Bewa, Buy, Bouchet, Szylit, & Sealy, 1982) (Zobel, 1998) (Kawabata, Sawayama, Nagashima, del Rosario, & Nakamura, 1984) (Franco, Ciacco, & Tavares, 1998) (Rosenthal, Nakamura, Espindola, & Jochimek, 1974) (van Soest, Hulleman, de Wilt, & Vliegthart, 1996). For starches, the native A- and B-type crystal lattices consist of double helical assembled in six-fold structures. The difference between the A- and B-type crystallinity is the packing density of the double helices in the unit cell. The double helices structures within the A- and B-type crystalline forms

are essentially the same, but the packing of the helices in the A-type crystalline structure is more compact than in the B-type crystallites, which have a more open structure with a hydrated core. The C-type crystal structure is believed to be a superposition of the A- and B- type crystal patterns. The C-type crystallites are thought to contain both types of polymorphs; The B-type polymorphs are in the center of the starch granules and are surrounded by the A-type crystal polymorphs (Wang, Yu, & Jin, 2008). Listed in Table 4.4 are the diffraction peaks and its intensity for the tapioca and sago starch. The corresponding d values of the diffraction peaks of tapioca and sago starch are also shown.

Table 4.4 Diffraction peaks and corresponding d values of tapioca and sago starch. The referral for intensity are vs = very strong, s = strong, m= medium and w = weak.

(Hoover & Sosulski, 1985) (Vansteelandt & Delcour, 1999) (Protserov, Karpov, Kozhevnikov, Wasserman, & Yuryev, 2000) (Bultosa & Taylor, 2003) (Bauer, Wiehle, & Dietrich, 2005) (Noosuk, Hill, Farhat, Mitchell, & Pradispenasena, 2005)

Angle (2θ) ($^{\circ}$)	d value (\AA)	Intensity
14.8	5.99	s
16.8	5.28	vs
17.1	5.19	vs
17.6	5.04	m
18.1	4.90	s
22.6	3.93	s
23.1	3.85	s
15.2	5.83	m
30.2	2.96	w
33.5	2.68	w

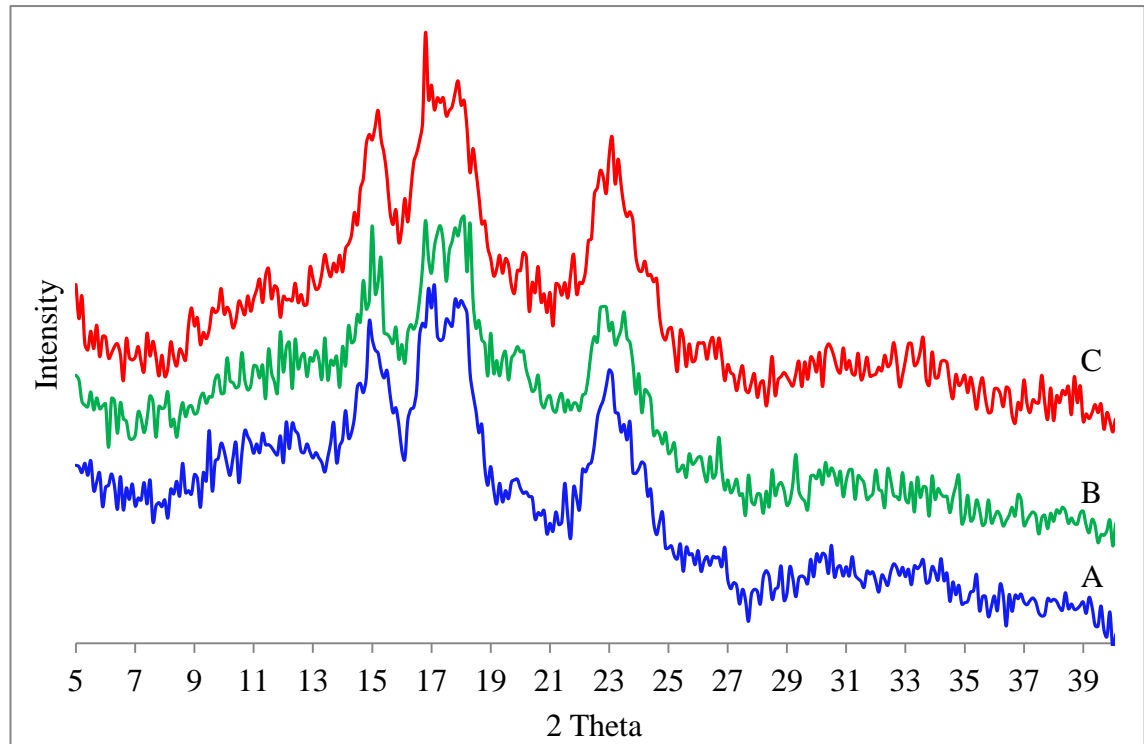


Fig. 4.20 X-ray diffractograms of tapioca (A), rice (B) and sago (C)

For rice starch, the diffraction peaks exhibited in the diffractogram resembles the A-type crystal pattern of starch. This is the typical crystal pattern for cereal starch (Pickard, Asaoka, & Blanshard, 1991) (Moorthy, Wenham, & Blanshard, 1996) (DeFloor, Dehing, & Delcour, 1998) (Galant, Bewa, Buy, Bouchet, Szylit, & Sealy, 1982) (Zobel, 1998) (Kawabata, Sawayama, Nagashima, del Rosario, & Nakamura, 1984) (Franco, Ciacco, & Tavares, 1998) (Rosenthal, Nakamura, Espindola, & Jochimek, 1974) (van Soest, Hullemann, de Wilt, & Vliegthart, 1996). Listed in Table 4.5 are the diffraction peaks and its intensity for rice starch. The corresponding d values of the diffraction peaks of rice starch are also shown.

Table 4.5 Diffraction peaks and corresponding d values of rice starch. The referral for intensity are vs = very strong, s = strong, m= medium and w = weak.

Angle (2θ) ($^{\circ}$)	d value (\AA)	Intensity
14.8	5.99	s
16.6	5.34	vs
17.7	5.01	s
18.1	4.90	s
22.8	3.90	vs
20	4.44	w
26.7	3.34	w
30.1	2.97	m
33.2	2.70	w

Figure 4.21 show the x-ray diffractograms for the four different types of treated fibers used in this study. For cellulose in a fiber, portions of it are arranged in an orderly fashion or lattice. The fundamental unit cell of cellulose as derived by Meyer and Misch is a monoclinic structure with three principal planes of reflection referred as (002), (101) and (10 $\bar{1}$) (Meyer & Misch, 1937). As mentioned in section 2.3.2.1, cellulose can exist in four polymorphs and between the four, cellulose I occur naturally and is the most abundant form found in nature. Cellulose I contains two existing phases that is cellulose I $_{\alpha}$ (triclinic) and cellulose I $_{\beta}$ (monoclinic) in varying proportions dependent on its botanical origin (Das & Chakraborty, 2006). From the diffractograms of the four treated fibers, the shape and the diffraction peaks observed are typical of cellulose I. The diffraction peaks of the treated fibers appears at $2\theta = 14.7^{\circ}$ (101), 16.1° (10 $\bar{1}$), 22.6° (002) and at 34.6° (040) (Parikh, Thibodeaux, & Condon, 2007) (Borysiak &

Doczekalska, 2005) (Mansikkamaki, Lahtinen, & Rissanen, 2007) (Ford, Mendon, Thames, & Rawlins, 2010) (Ago, Endo, & Hirotsu, 2004).

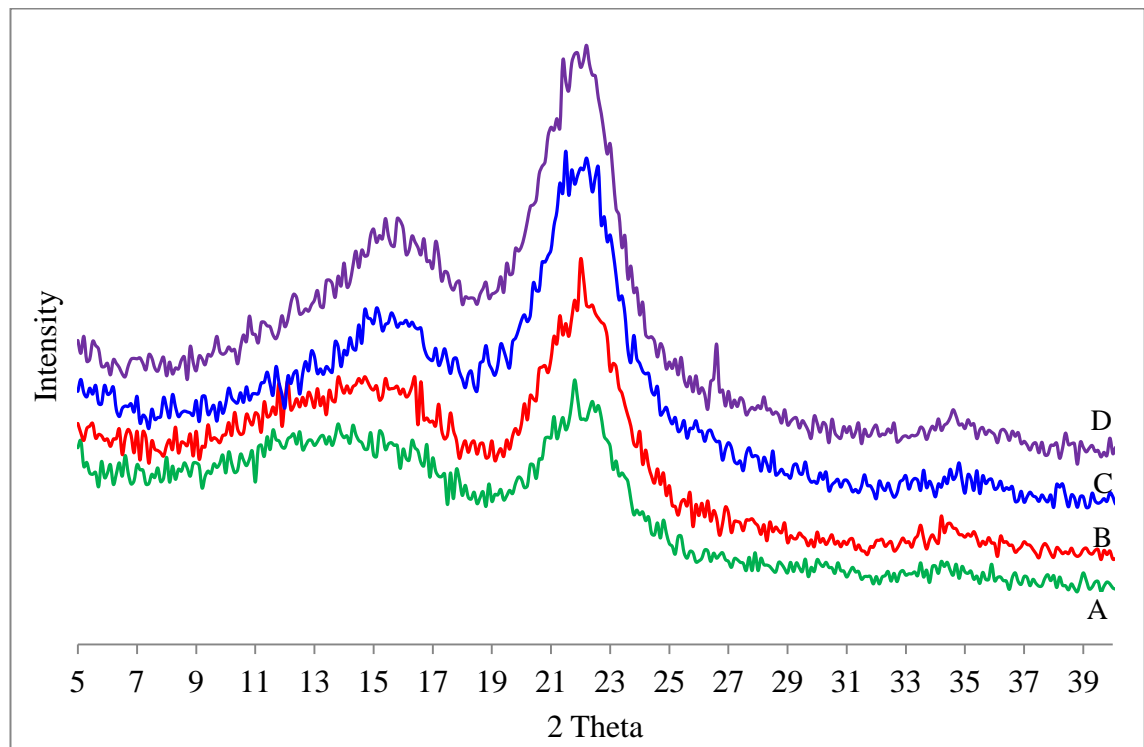


Fig. 4.21 X-ray diffractograms of treated roselle (A), kenaf (B), bamboo (C), and Napier (D).

Even though the mercerization process of a fiber can change the cellulose polymorph form from cellulose I to cellulose II, it was not the objective of this study to change the polymorph of the four natural fibers used. The main purpose on why the mercerization and bleaching process was done on the natural fibers was to remove the natural and artificial impurities such as hemicellulose, pectin, lignin, waxes and oils and by doing so increases the effective area available for contact with the starch and polymer matrix. The removal of the impurities will also leave a major number of hydroxyl groups on the cellulose so that it is accessible for the starch and polymer matrix to develop links and will result in better interlocking between different components in the composite. Low concentration of sodium hydroxide (NaOH) ($< 15\%$) in the mercerization process will

solubilise the impurities without changing the cellulose crystalline polymorph (Borysiak & Doczekalska, 2005) (Oh, et al., 2005). Another factor that contributes to the possible explanation on why there was no structural change in the cellulose may be in the presence of lignin in the treated fibers. Basically, the process of mercerization starts in the amorphous portion of the fiber and proceeds to the crystalline region of cellulose. The presence of lignin may prevent the alkali swelling of cellulose because it prevents the Na⁺ ions from reaching the deeper part of the crystal lattice and this indirectly hinders the polymorph's transformation. In the FTIR spectrum of the four treated fibers, lignin was detected in the 1465 -1608 cm⁻¹ range and due to the low concentration of NaOH used in the mercerization process; the treated fibers exhibited only partial delignification. The evidence of the removal of impurities such as hemicellulose can be seen in the FTIR spectrum of the four treated fibers (Figure 4.3) where the absorption peak of hemicellulose between the ranges of 1720-1745 cm⁻¹ cannot be detected (Sun & Sun, 2002). Table 4.6 shows estimations of the crystallinity index of the four treated fiber used in the study. The crystallite widths of the four treated natural fibers are also shown. The estimation of the crystallinity index and the crystallite width calculated for the different treated fibers used did not vary much in values. This directly shows that the crystallinity of cellulose in the four treated fibers is nearly the same.

Table 4.6 The crystallinity indexes and the crystallite width of four treated fibers

Fibers	Crystallinity Index (%)	Crystallite Width (Å)
Bamboo	56.35	19.32
Kenaf	54.62	19.46
Roselle	50.48	19.74
Napier	52.68	17.49

PVA/different starches composites

Figure 4.22, 4.23 and 4.24 show the x-ray diffractograms of PVA blended with different concentration of starches. The diffraction patterns of the blended polymer and starches were compared with the diffraction pattern of pure PVA and pure tapioca starch.

In the blended films of PVA with different concentration of different starches, most of the diffraction peaks that reflect the crystalline regions in the starch were not detected and that the diffraction patterns of the diffractograms were very similar to that of neat PVA. Listed in Table 4.7 are the crystallite widths for the composite of PVA blended with different concentration of different starches. From the values listed in Table 4.7, the crystallite width of the blended films decreases as the content of starch added to the blended films increases. The decreased in crystallite width may indicate that the crystal structure of PVA was changed. When forming the blended films, the interface bonding may result in the increase in the number of intermolecular hydrogen bonding between starch and PVA and this indirectly decreases the crystallite width of the components in the blended films. The decreased in the crystallite size may also be attributed to the decreased in the crystallinity of the blended composite, leading to an amorphous structure being formed.

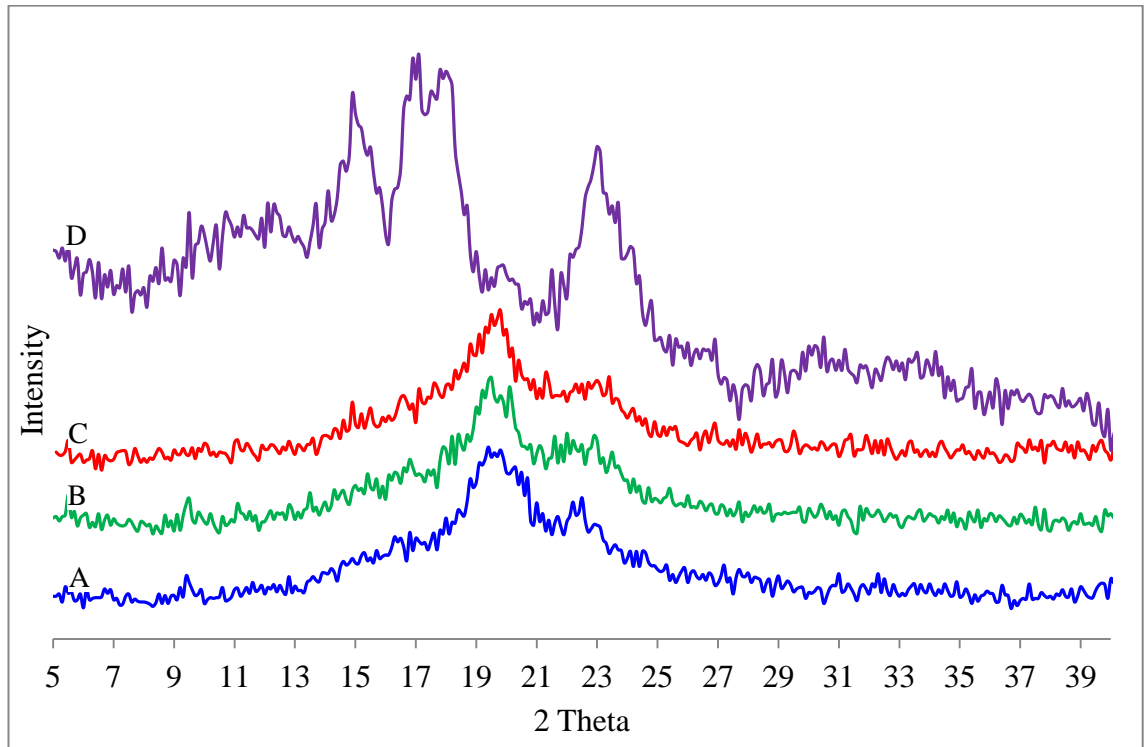


Fig. 4.22 X-ray diffractograms of pure PVA (A), PVA/1TS (B), PVA/3TS (C) and pure tapioca starch (D)

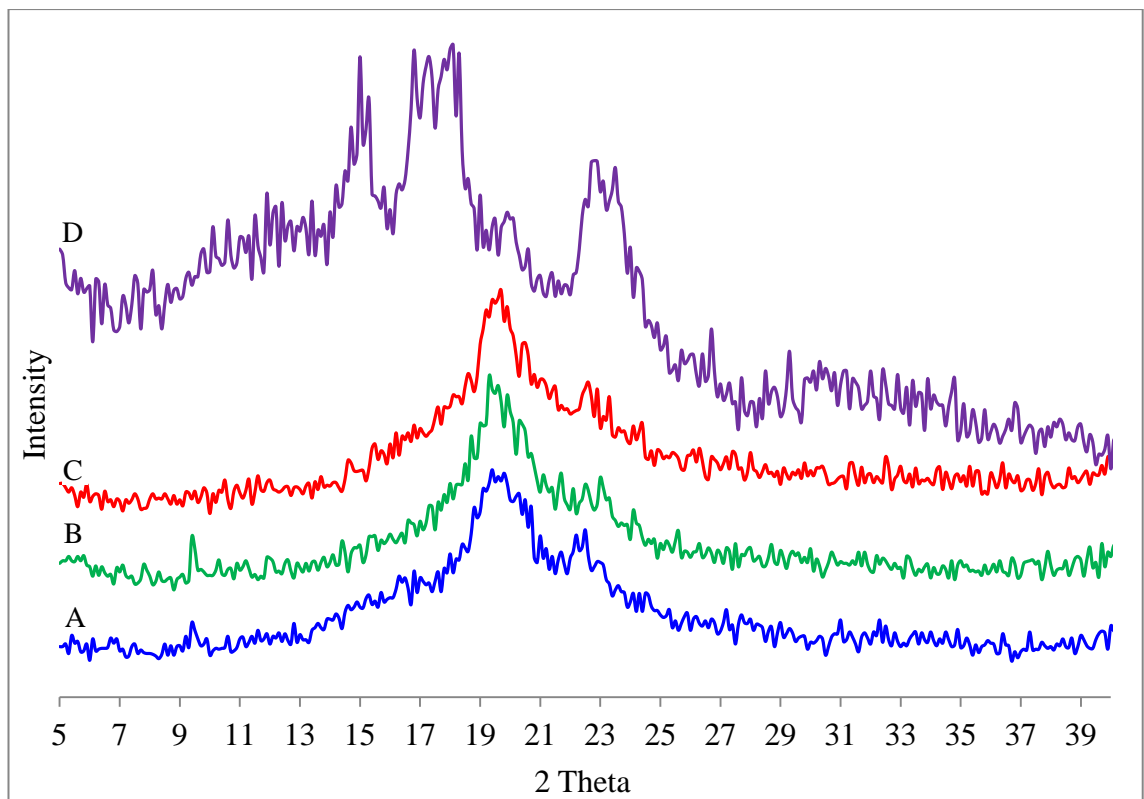


Fig. 4.23 X-ray diffractograms of pure PVA (A), PVA/1RS (B), PVA/3RS (C) and pure rice starch (D)

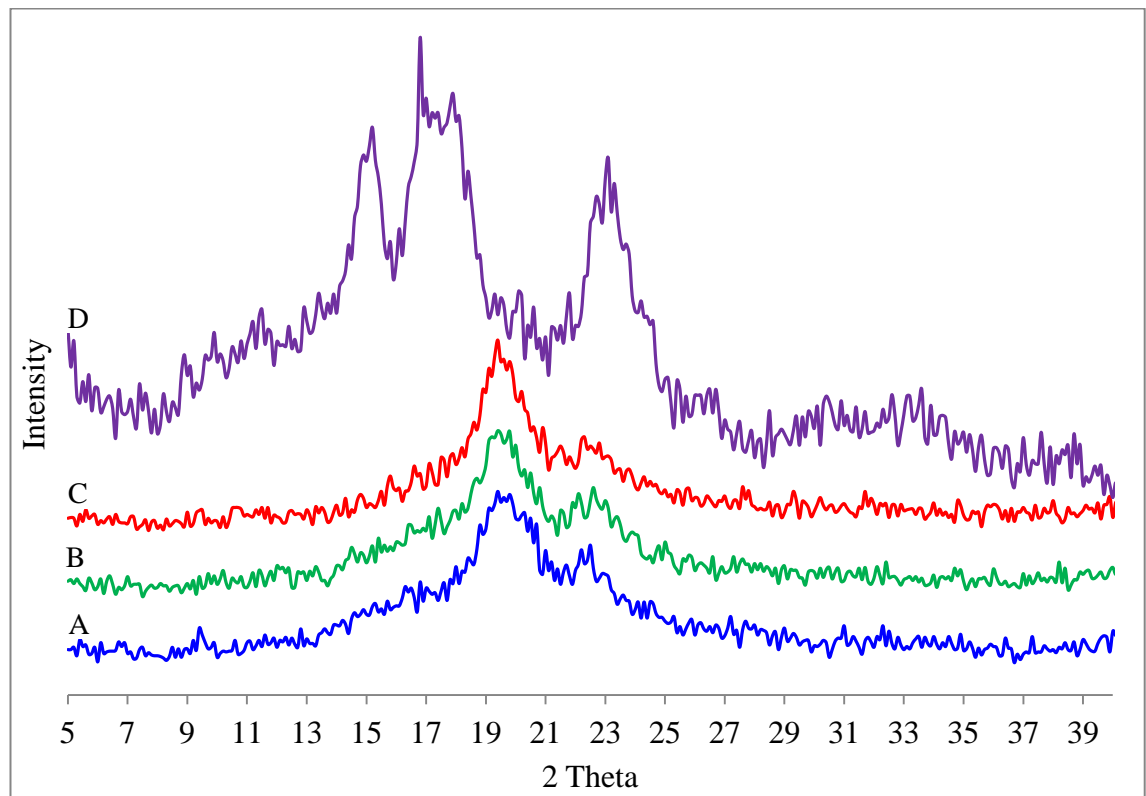


Fig. 4.24 X-ray diffractograms of pure PVA (A), PVA/1SS (B), PVA/3SS (C) and pure sago starch (D)

Table 4.7 The crystallite width of PVA blended with different concentration of different starches

Samples	Crystallite Width (Å)	Samples	Crystallite Width (Å)	Samples	Crystallite Width (Å)
PVA/1TS	23.37	PVA/1RS	32.90	PVA/1SS	35.04
PVA/3TS	18.54	PVA/3RS	29.86	PVA/3SS	26.88

PVA/different starches/different fibers composites

Figure 4.25, 4.26, 4.27 and 4.28 shows the x-ray diffractograms of PVA blended with 1g tapioca starch and different concentration of different treated fibers.

Figure 4.29, 4.30, 4.31 and 4.32 shows the x-ray diffractograms of PVA blended with 1g of rice starch and different concentration of different treated fibers.

Figure 4.33, 4.34, 4.35 and 4.36 shows the x-ray diffractograms of PVA blended with 1g of sago starch and different concentration of different treated fibers.

Listed in Table 4.8 are the crystallite widths for the composite of PVA blended with 1g of different starches and mix with different concentration of different treated fibers.

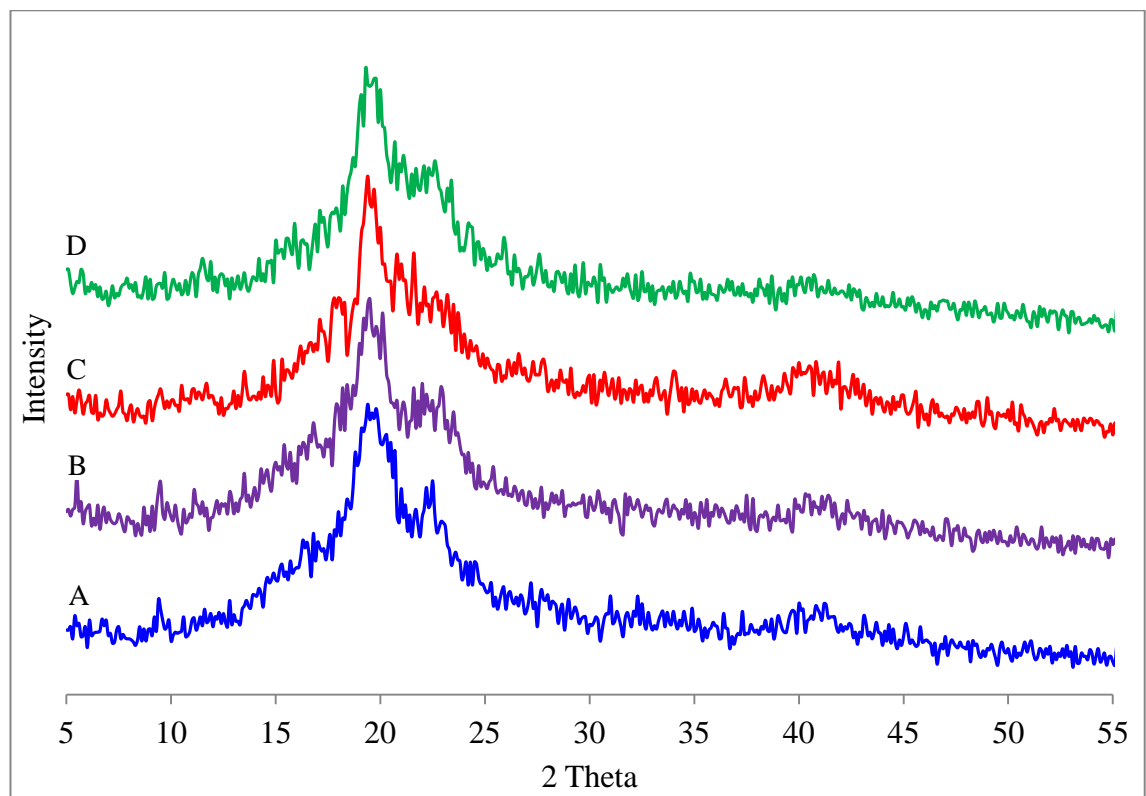


Fig. 4.25 X-ray diffractograms of pure PVA (A), PVA/1TS (B), PVA/1TS/1BB (C) and PVA/1TS/3BB (D)

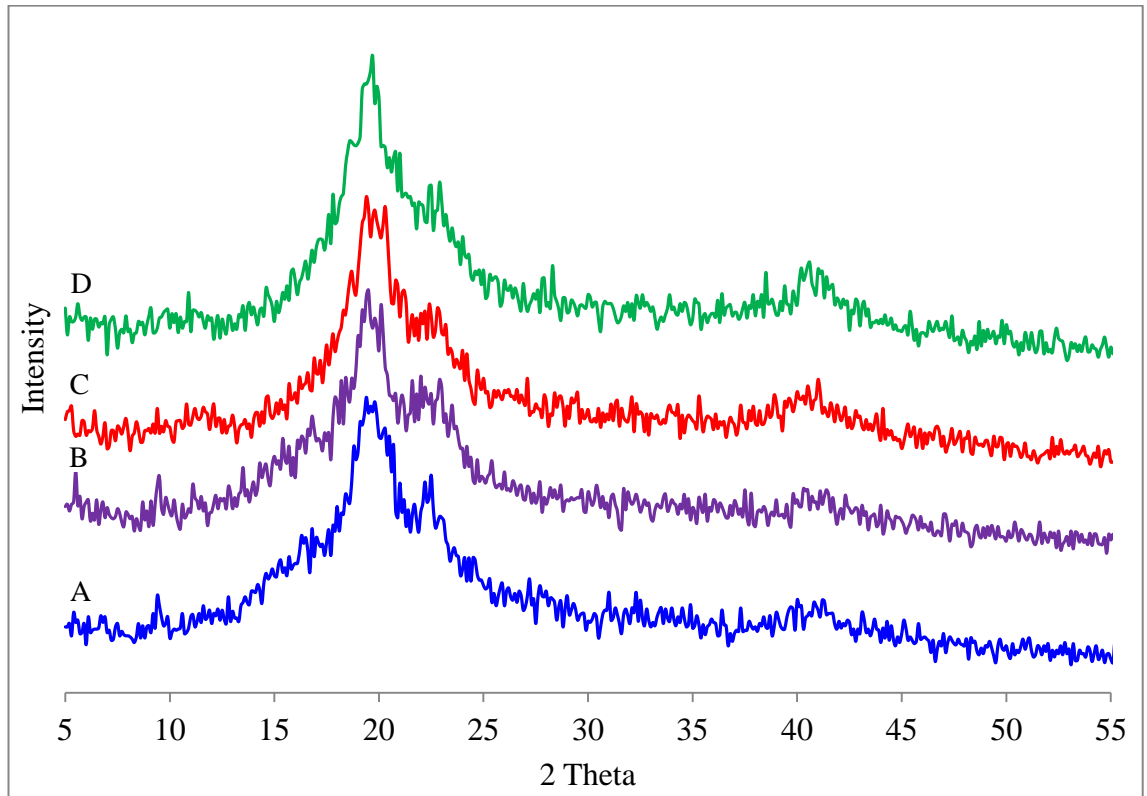


Fig. 4.26 X-ray diffractograms of pure PVA (A), PVA/1TS (B), PVA/1TS/1KF (C) and PVA/1TS/3KF (D)

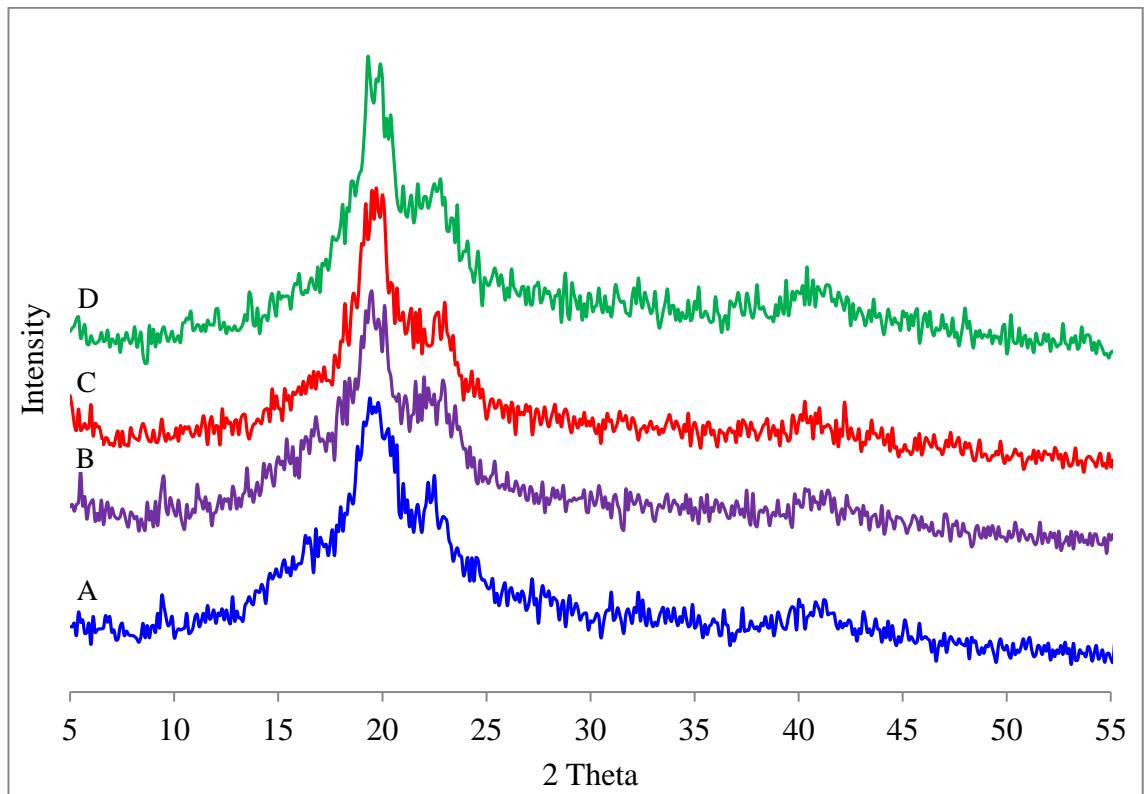


Fig. 4.27 X-ray diffractograms of pure PVA (A), PVA/1TS (B), PVA/1TS/1ROS (C) and PVA/1TS/3ROS (D)

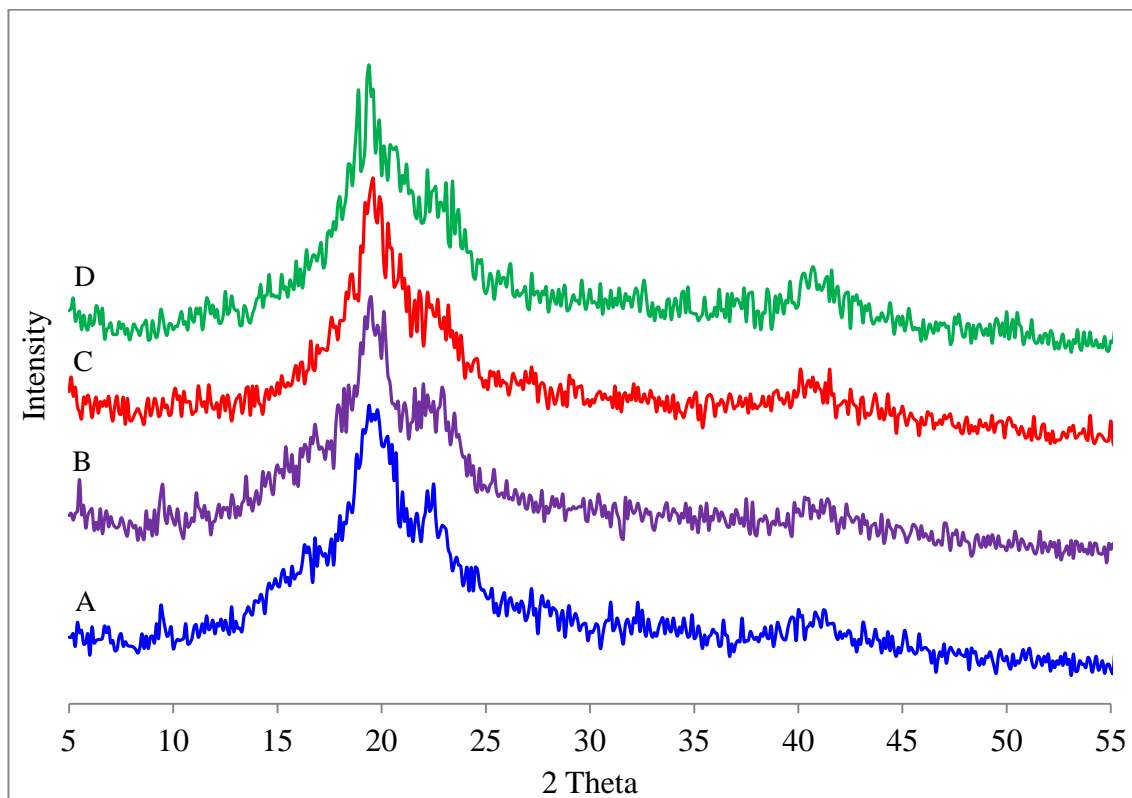


Fig. 4.28 X-ray diffractograms of pure PVA (A), PVA/1TS (B), PVA/1TS/1NP (C) and PVA/1TS/3NP (D)

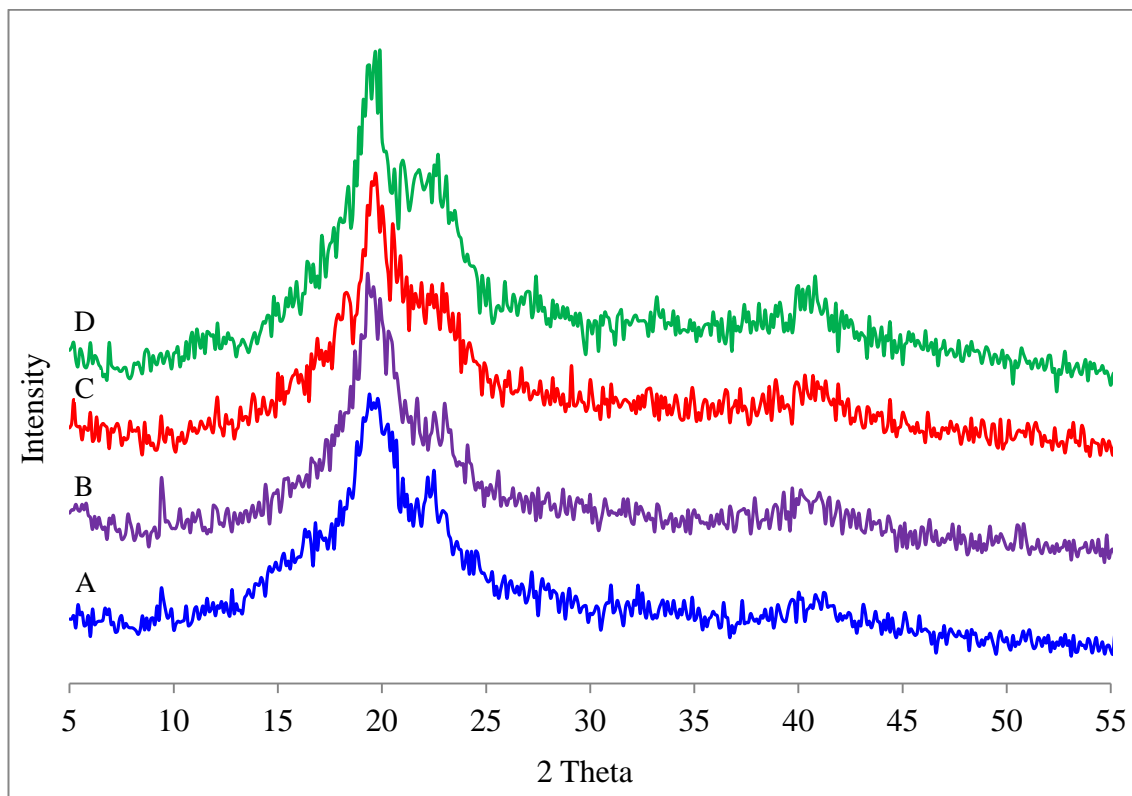


Fig. 4.29 X-ray diffractograms of pure PVA (A), PVA/1RS (B), PVA/1RS/1BB (C) and PVA/1RS/3BB (D)

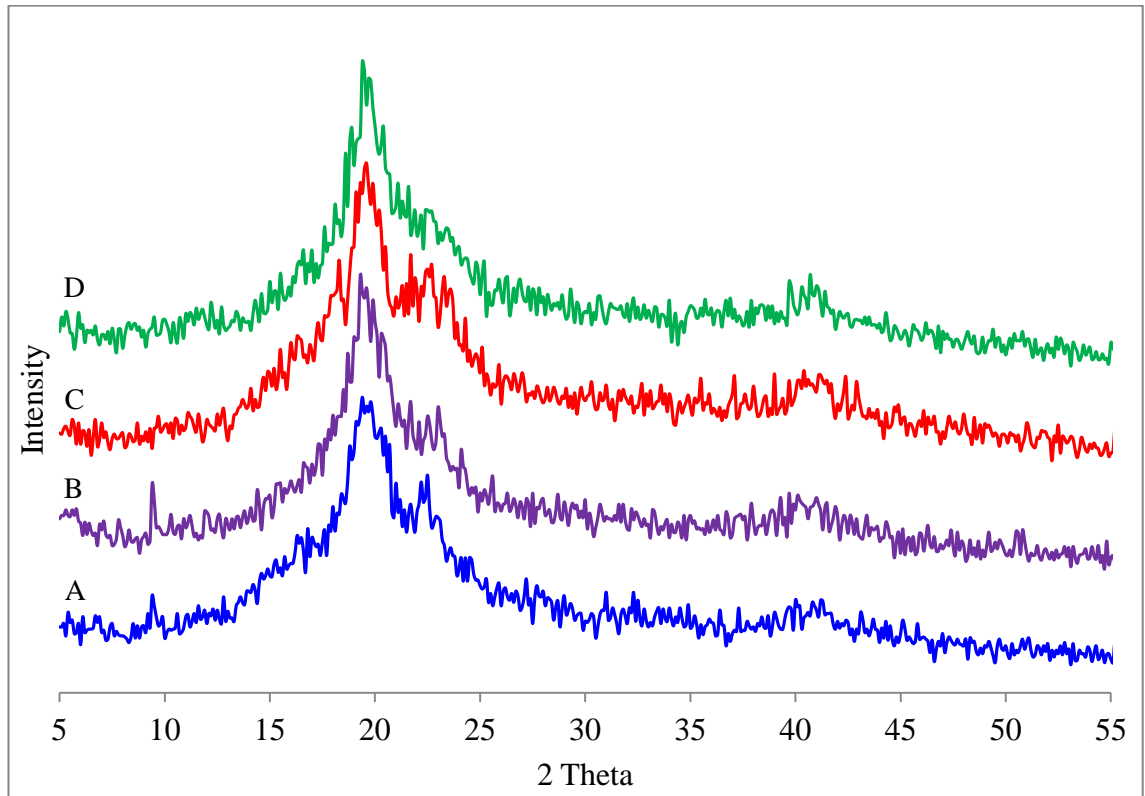


Fig. 4.30 X-ray diffractograms of pure PVA (A), PVA/1RS (B), PVA/1RS/1KF (C) and PVA/1RS/3KF (D)

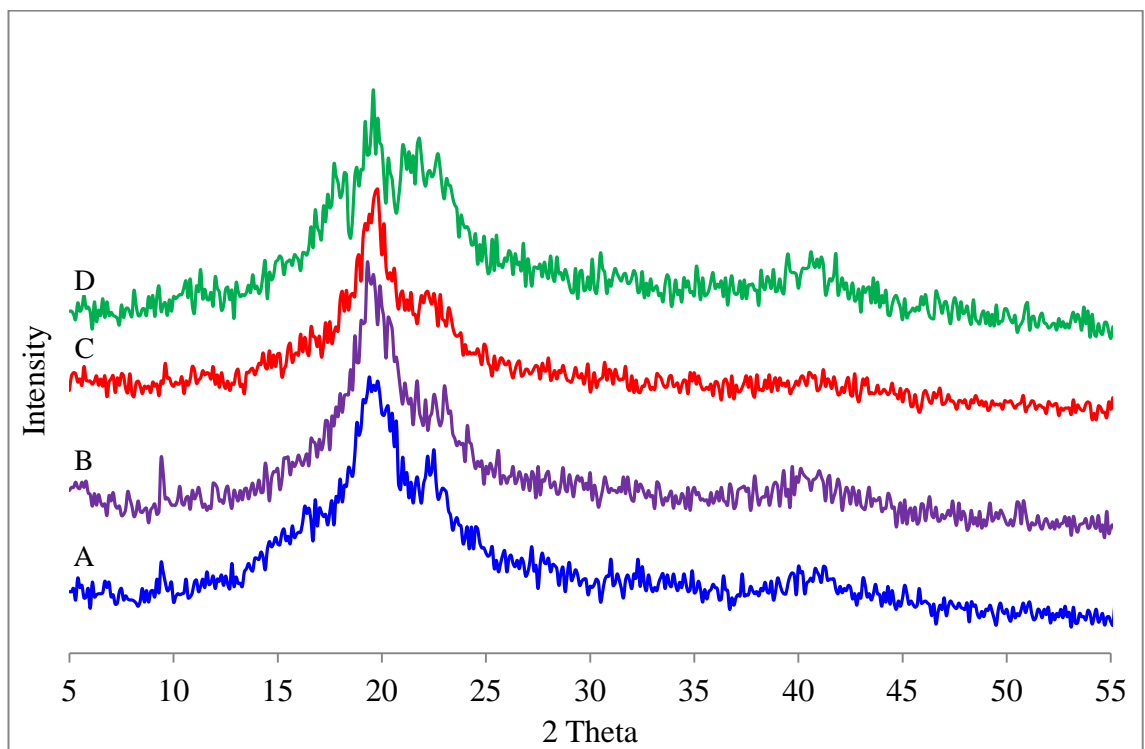


Fig. 4.31 X-ray diffractograms of pure PVA (A), PVA/1RS (B), PVA/1RS/1ROS (C) and PVA/1RS/3ROS (D)

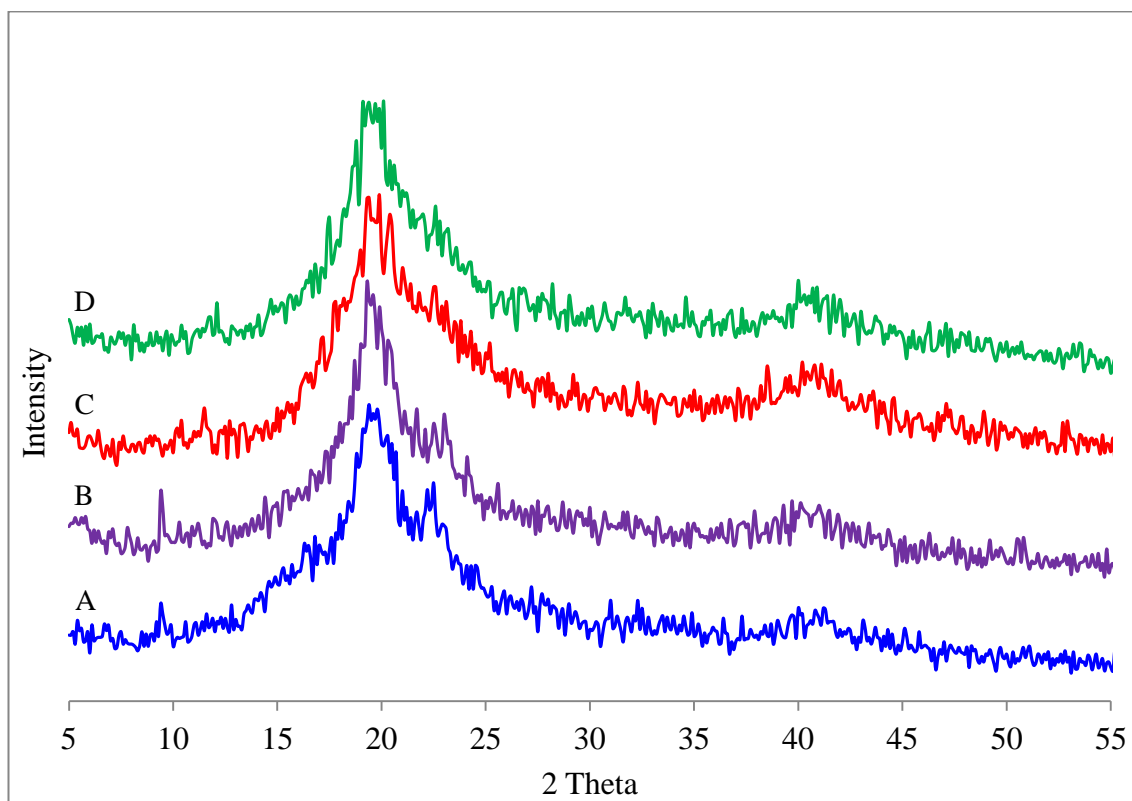


Fig. 4.32 X-ray diffractograms of pure PVA (A), PVA/1RS (B), PVA/1RS/1NP (C) and PVA/1RS/3NP (D)

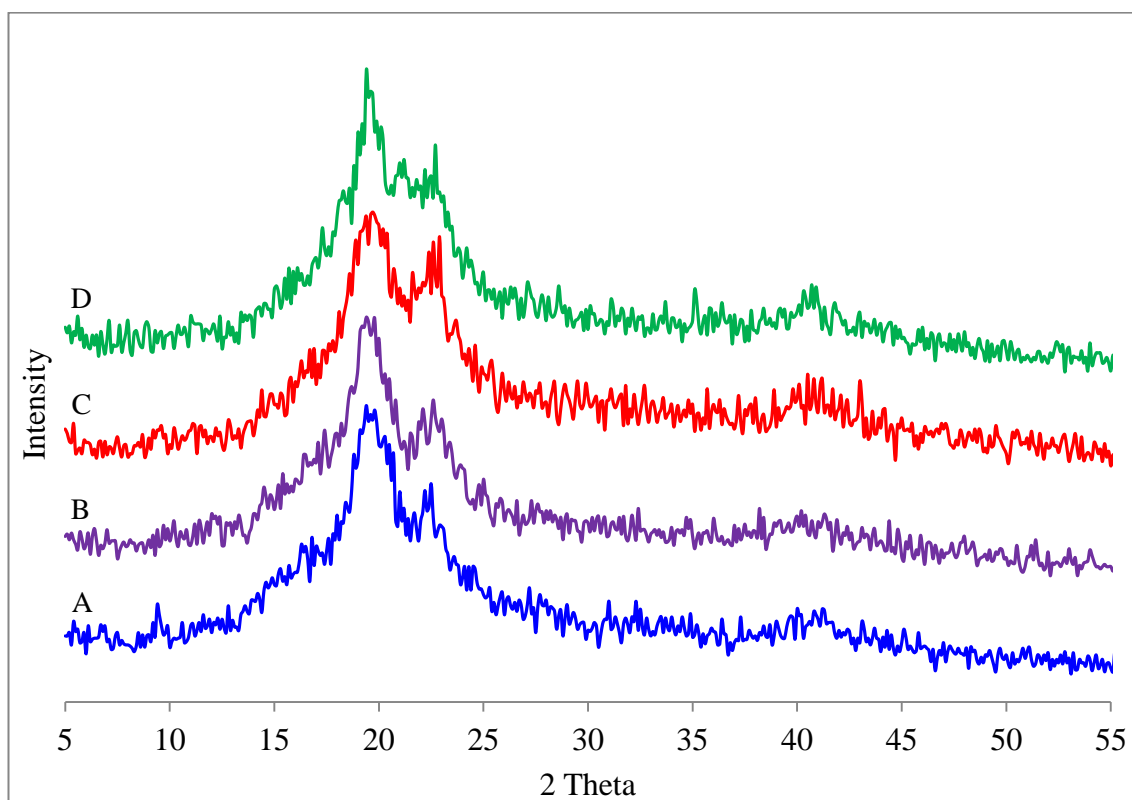


Fig. 4.33 X-ray diffractograms of pure PVA (A), PVA/1SS (B), PVA/1SS/1BB (C) and PVA/1SS/3BB (D)

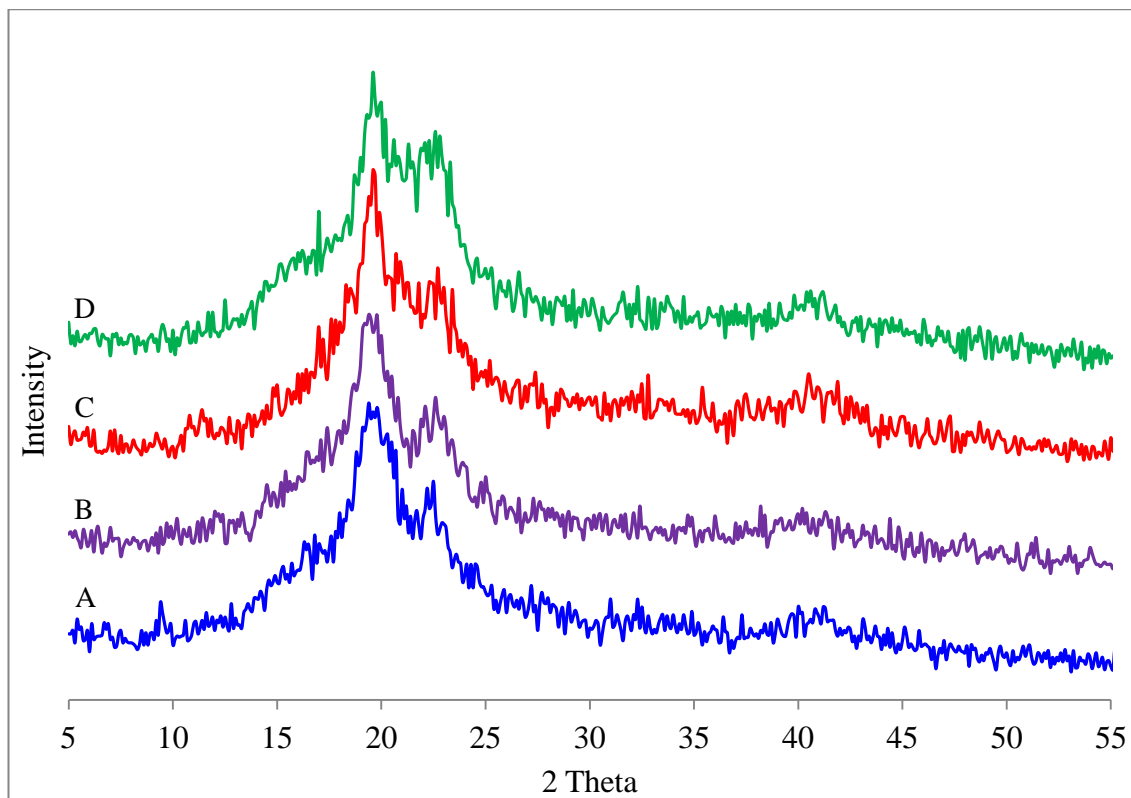


Fig. 4.34 X-ray diffractograms of pure PVA (A), PVA/1SS (B), PVA/1SS/1KF (C) and PVA/1SS/3KF (D)

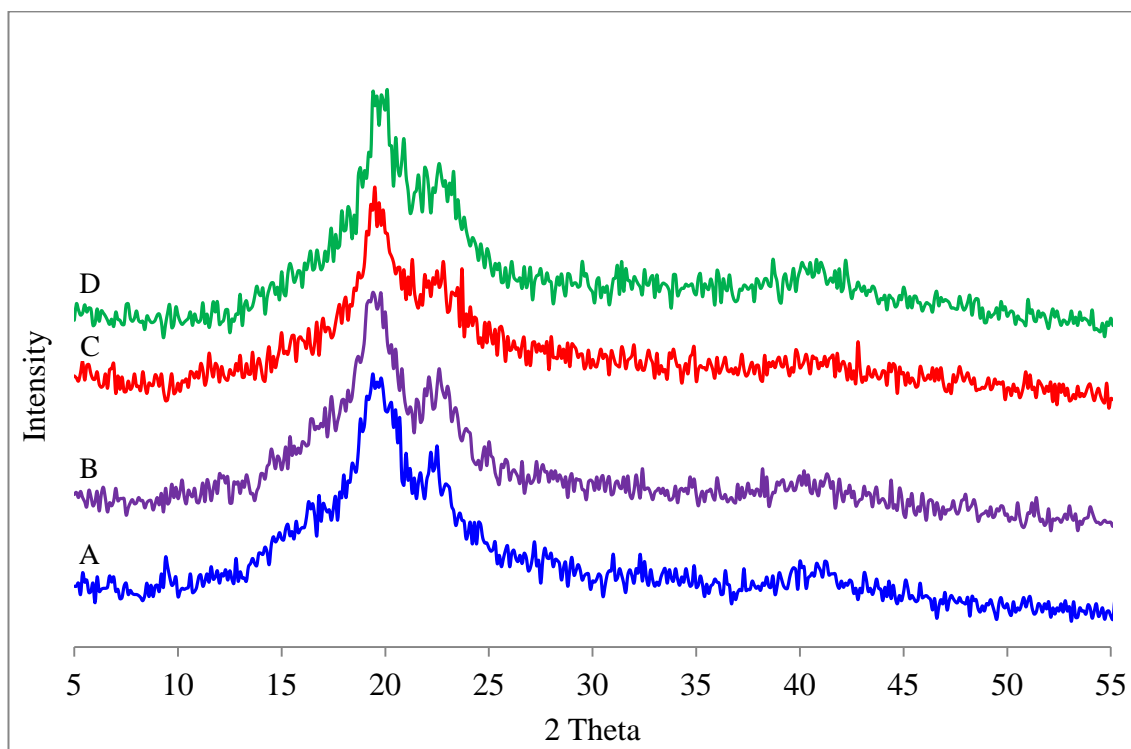


Fig. 4.35 X-ray diffractograms of pure PVA (A), PVA/1SS (B), PVA/1SS/1ROS (C) and PVA/1SS/3ROS (D)

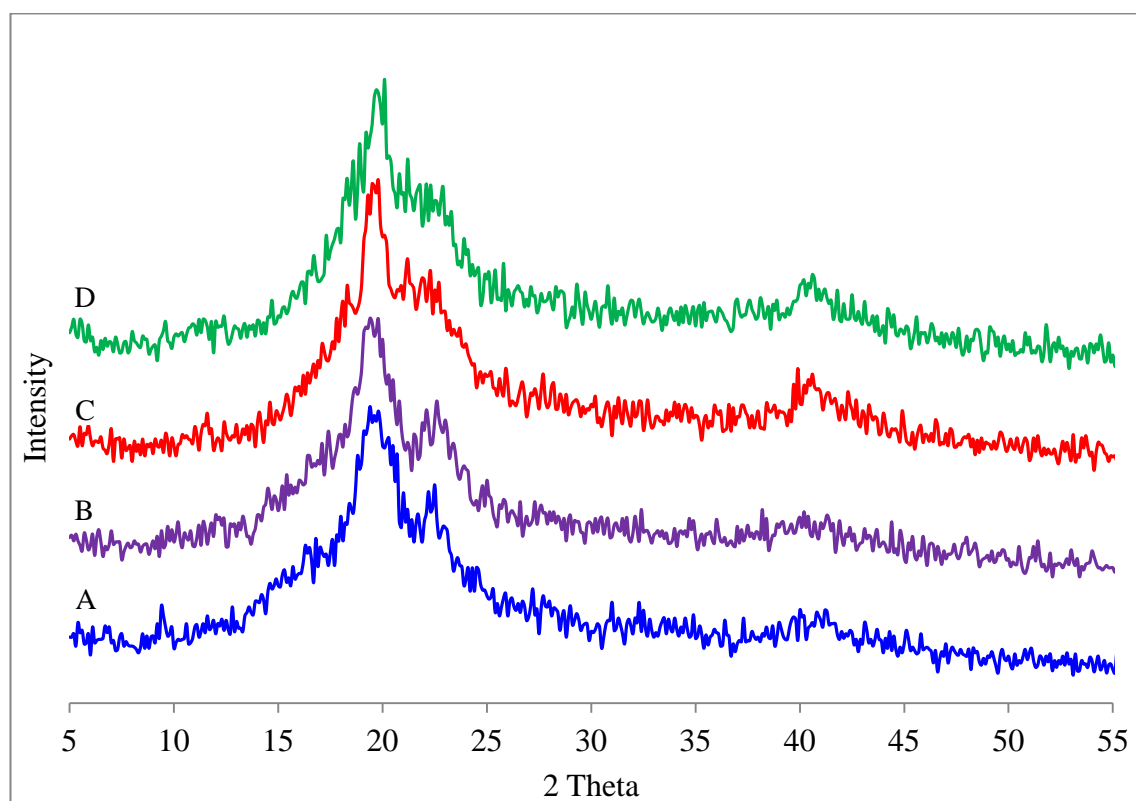


Fig. 4.36 X-ray diffractograms of pure PVA (A), PVA/1SS (B), PVA/1SS/1NP (C) and PVA/1SS/3NP (D)

Table 4.8 The crystallite widths of PVA blended with 1g of different starches with different concentration of different treated fibers

Composite	Crystallite Width (Å)	Composite	Crystallite Width (Å)
PVA/1TS/1BB	30.42	PVA/1TS/3BB	23.03
PVA/1TS/1KF	32.25	PVA/1TS/3KF	29.86
PVA/1TS/1ROS	26.88	PVA/1TS/3ROS	26.01
PVA/1TS/1NP	30.42	PVA/1TS/3NP	29.85
PVA/1RS/1BB	28.29	PVA/1RS/3BB	25.59
PVA/1RS/1KF	29.86	PVA/1RS/3KF	27.80
PVA/1RS/1ROS	35.84	PVA/1RS/3ROS	29.86
PVA/1RS/1NP	32.25	PVA/1RS/3NP	31.01

PVA/1SS/1BB	26.01	PVA/1SS/3BB	24.43
PVA/1SS/1KF	29.86	PVA/1SS/3KF	27.80
PVA/1SS/1ROS	23.37	PVA/1SS/3ROS	22.39
PVA/1SS/1NP	29.86	PVA/1SS/3NP	27.80

Observation on the result of the diffractograms show that the composites with treated fibers exhibited basically the same crystalline pattern when compared with the blend of PVA and starch, but with a slight appearance of a shoulder for 2θ values between 21° and 23° , which is associated with the addition of crystalline treated fibers (Tomczak, Sydenstricker, & Satyanarayana, 2007). The weakening of the 2θ peak at 19.6° and the decreasing crystallite width in the blend of composite with fibers as the fiber content increases are due to the formation of a more amorphous phase in the blended composite. The blending of PVA and starch may attribute to partial destruction of the starch crystalline phase and this may lead to an amorphous structure being formed. The blending also induces co-crystallization between PVA, starch and cellulose and a more disordered crystalline phase may be formed in the composite